Nano Energy 70 (2020) 104546

Contents lists available at ScienceDirect

Nano Energy

journal homepage: http://www.elsevier.com/locate/nanoen

Full paper

Ultra-stretchable triboelectric nanogenerator as high-sensitive and self-powered electronic skins for energy harvesting and tactile sensing

Kangkang Zhou [a], Yi Zhao [a], Xiupeng Sun [b], Zuqing Yuan [c], Guoqiang Zheng [a], Kun Dai [a,*], Liwei Mi [d], Caofeng Pan [c,**], Chuntai Liu [a], Changyu Shen [a]

[a] School of Materials Science and Engineering, Key Laboratory of Materials Processing and Mold (Zhengzhou University), Ministry of Education, National Engineering Research Center for Advanced Polymer Processing Technology, Zhengzhou University, Zhengzhou, 450001, China
[b] MOE Key Laboratory of Materials Physics, School of Physics and Engineering, Zhengzhou University, Zhengzhou, 450001, China
[c] Beijing Institute of Nanoenergy and Nanosystems, Chinese Academy of Sciences, National Center for Nanoscience and Technology (NCNST), Beijing, 100083, China
[d] School of Materials and Chemical Engineering, Zhongyuan University of Technology, Zhengzhou, Henan, 451191, China

ARTICLE INFO

Keywords:
Stretchable triboelectric nanogenerator
Graphene
Silver nanowires
Thermoplastic polyurethane
Self-powered electronic skins

ABSTRACT

Rapid development of wearable electronic devices stimulates various requirements for power supply devices, such as sustainability, maintenance-free and stretchability. Herein, we fabricate a flexible and self-powered electronic skin (e-skin) based on an ultra-stretchable triboelectric nanogenerator (STENG) by multilayered thermoplastic polyurethane (TPU)/silver nanowires (AgNWs)/reduced graphene oxide (rGO). Due to the ultra-stretchable property of the TPU fibrous mats and the synergistic effect of the multilayered AgNWs/rGO microstructure, our e-skin demonstrates excellent stability and high stretchability (200% strain). The e-skin (2×2 cm^2) delivers a high open-circuit voltage (202.4 V) and a large instantaneous power density (6 mW/m^2), which can be used as an efficient energy supply device. Whereas, our e-skin possesses a high sensitivity (78.4 kPa^{-1}) and a fast response time (1.4 ms) towards pressure, demonstrating its excellent tactile sensing capability. On the basis of the excellent performances, the e-skin can sense strength and trajectory of motion of the mechanical stimulus, clear and accurate results have been obtained. The results provide a new and practical strategy for fabricating STENG based high performance and self-powered e-skin for soft robots, human-machine interaction and internet of things.

1. Introduction

Intelligent wearable electronic devices have been developed rapidly owing to its wide prospects in movement monitoring, internet of things and human-machine interaction, etc [1–7]. Wearable electronic skin (e-skin) is widely concerned because of their large stretchability, high sensitivity and excellent skin affinity [8–12]. In previous reports, e-skins usually require a power connection or a battery to provide power, which severely limits the applicability and life span of e-skins, and raises maintenance and recharging costs more or less [13–15]. To improve the wearable comfort of e-skins, the energy supply devices of e-skins should be stretchable, which can fit tightly to human skin and deform following the body motions [16]. Therefore, stretchable, sustainable, lightweight and environmentally friendly power supplies remain a key issue for e-skins [17–19]. In order to satisfy the requirements of next-generation e-skin, highly sensitive, ultra-stretchable, comfortable and self-powered sensing system is urgently needed [20].

In recent years, triboelectric nanogenerator (TENG), which works by contact electrification and electrostatic induction [21–27], has been proved to have excellent performance in various energies harvesting and signal collection [28–33]. The TENG possesses the advantages of light weight and is simple in structure; energy generated by low-frequency movement of human body can also be collected by TENG, which provides a new solution for energy supply of e-skin [34]. TENG can also serve as a fast response, highly sensitive self-powered sensor that could convert mechanical signals into electrical signals efficiently [35]. A wide range of materials can be applied to fabricate TENG as triboelectric layer (such as various flexible polymers) and electrode (such as hydrogel, metal), which greatly expands its potential applications. To meet the new demand for e-skins, it is undoubtedly appealing and necessary to

* Corresponding author.
** Corresponding author.
E-mail addresses: kundai@zzu.edu.cn (K. Dai), cfpan@binn.cas.cn (C. Pan).

https://doi.org/10.1016/j.nanoen.2020.104546
Received 18 December 2019; Received in revised form 12 January 2020; Accepted 28 January 2020
Available online 1 February 2020

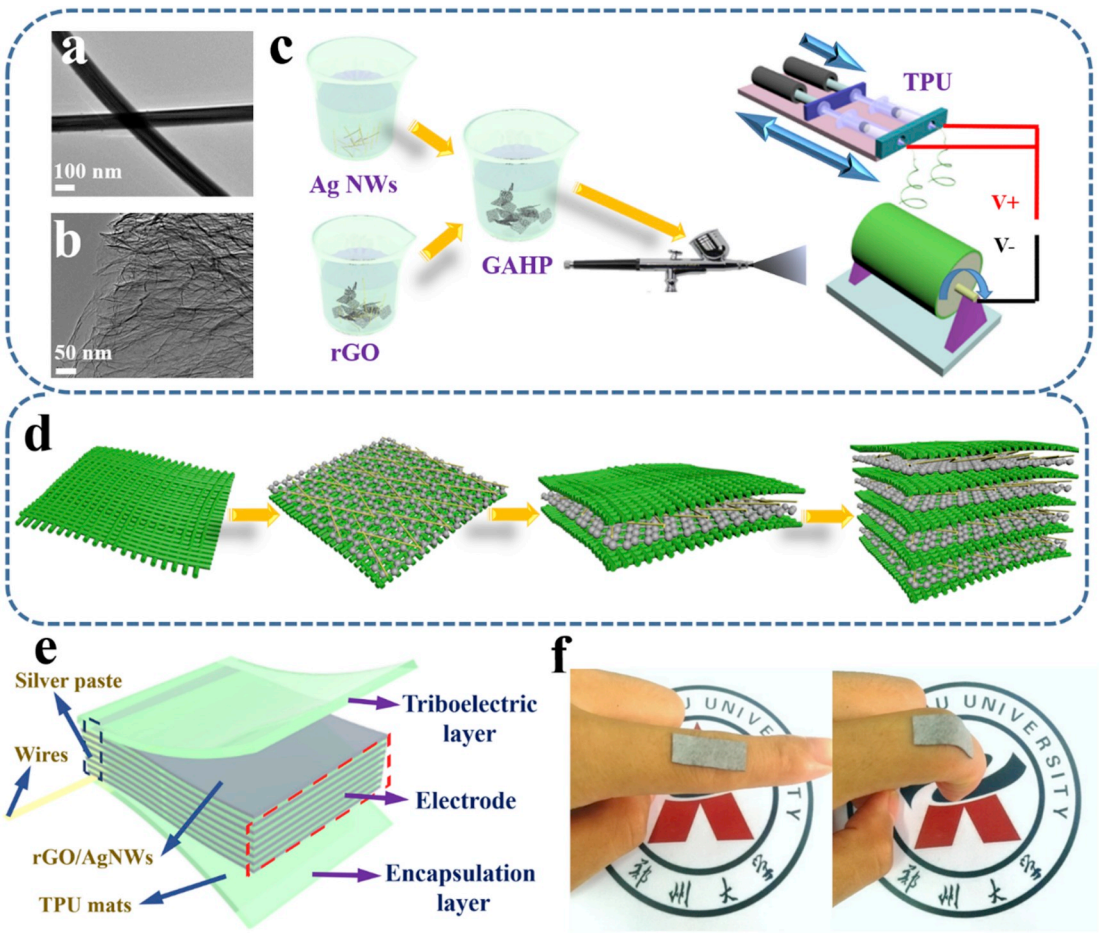

Fig. 1. TEM images of AgNWs (a) and rGO (b). (c) The preparation process and equipment diagram for fabricating e-skin. (d) The forming process of e-skin with rGO and AgNWs as conductive fillers. (e) The schematic structure of our STENG based e-skin. (f) Real photograph of e-skin on a finger.

empower wearable devices with the capabilities of energy-harvesting and sensing in terms of realizing self-powered devices [36].

As a new generation of e-skin, stretchability is crucial [37–40]. Stretchable TENG (STENG) based e-skin has been used as wearable power supplies and self-powered sensors, such as motion monitor, respiratory sensors and touch sensors [41–47]. In previous reports, STENG based e-skins were primarily composed of flexible polymers due to their high elongation at break (strain>100%), such as polydimethylsiloxane (PDMS) and Eco-flex [48,49]. While airtight PDMS STENG based e-skins are hydrophobic and air proof, which may cause discomfort and irritation for the human skin in long-term use [50]. Recently, the stretchable fibrous mats prepared by the electrospinning with porosity, breathability and large surface area, has shown great advantages in wearable comfort and triboelectric properties [51–53].

On the other hand, electrode materials with stretchable properties are also important for fabricating STENG [54]. Highly stretchable conductive hydrogel with added ions or conductive materials are widely used as stretchable electrodes for STENG [55]. However, hydrogels always lose their stability and conductivity because of the dehydration phenomenon over time. Silver nanowires (AgNWs) have been considered as ideal conductive layers for STENG based e-skin on the basis of their controllable nanostructures, large aspect ratio, outstanding electrical properties and mechanical properties [56]. Despite these efforts, roadblocks still exist in developing the ideal conductive layers of STENG based e-skins with excellent charge transfer performance, even for the most promising AgNWs. AgNWs will slip to each other under a large mechanical deformation, the STENG based e-skins thus tend to suffer from considerable electrical output variation (instability), which limits its wide application. To address this instability and strengthen the connection between AgNWs, it is necessary to introduce another conductive nanomaterial into the AgNWs conductive network. The two-dimensional reduced graphene oxide (rGO) sheets have high conductivity and large specific surface area, which can be used to build an excellent conductive network. Due to the ultrathin structure (about 0.8 nm) of rGO (Fig. S1), it could reduce the thickness and improves the flexibility of the conductive layer.

In this work, we prepared a highly stretchable TENG based e-skin with designed multilayered flexible fibrous mats and AgNWs/rGO synergic conductive network. The rGO was used to construct a synergic conductive network with AgNWs to prepare stretchable electrodes for the STENG based e-skin. Thermoplastic polyurethane (TPU) was selected as the triboelectric and protection layers on the basis of its strong electronegativity and excellent flexibility. The TPU fibrous mats with high stretchability, breathability and light mass were fabricated by electrospinning. rGO and AgNWs were sprayed on the TPU mats layer by layer during the electrospinning to construct stable conductive paths separately. The open-circuit voltage, instantaneous power density, sensitivity and response time towards pressure of the STENG based e-skin (2×2 cm^2) were measured to evaluate the sensing performances. The tactile sensing behaviors in self-powered manner were also investigated. Results show that our e-skin could maintain stable output and sensing performance even if it was stretched to a very large deformation (200% strain). Furthermore, an e-skin array (5×5) was assembled for touch sensing test on the basis of its excellent stretchability, light weight and high sensitivity, showing broad applications in human-machine interaction and soft robots.

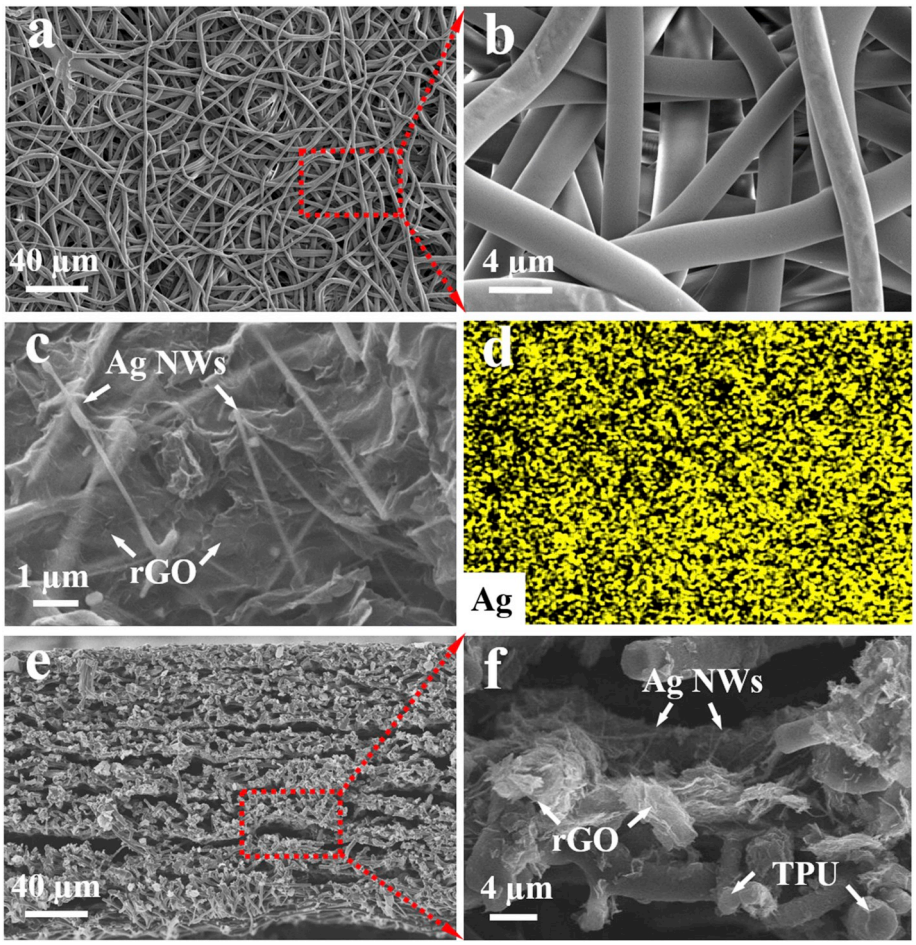

Fig. 2. SEM images of rGO/AgNWs/TPU e-skin. (a, b) SEM images of surface of the e-skin at various magnification. SEM (c) and EDS mapping (d) images of rGO/AgNWs conductive layer. (e, f) SEM images of cross section of the e-skin at different magnification.

2. Experimental section

2.1. Fabrication of the AgNWs

AgNWs were prepared by reducing silver nitrate (Sinopharm Chemical Reagent Co., Ltd., China.) in ethylene glycol (EG, Fuyu Fine Chemical Co. Ltd, Tianjin, China) with the addition of polyvinylpyrrolidone (PVP, BASF Co. Ltd.). Firstly, $AgNO_3$ (204 mg) and PVP (399.6 mg) were added into EG (20 mL) simultaneously in a flask, the solution was evenly dispersed in a dark environment. Sodium chloride (NaCl, Zhiyuan Reagent Co. Ltd., Tianjin, China.) solution with 0.1 M in EG was configured, then it (10 μL) was added into the flask. Finally, the flask was heated to 170 °C, 1 h later, AgNWs would be synthesized. To remove PVP and EG, the solution was washed by ethanol for three times.

2.2. Fabrication of rGO and AgNWs hybrid particles (GAHP)

5 mg rGO (Suzhou TanFeng Graphene Science and Technology Co. Ltd., China) was dispersed in ethanol under ultrasonic treatment for 1 h 5 mg AgNWs were added into the rGO solution at a certain concentration, the mixed solution was stirred for 30 min to achieve a homogeneous dispersion. Finally, the GAHP was prepared for further experiments.

2.3. Fabrication of self-powered STENG based e-skin

E-skin was fabricated by electrospinning and spraying alternately. Firstly, a solution was prepared by adding 5 g TPU pellets (code Elastollan 1185A, BASF Co. Ltd.) into a mixed solvent of 10 mL N, N-Dimethylformamide and 10 mL tetrahydrofuran (the concentration was 0.25 g/mL) (DMF and THF, Zhiyuan Reagent Co. Ltd., Tianjin, China.). The solution was moved into two 10 mL plastic syringes with curved metal nozzles, which were connected to a voltage of 26 kV. A rotating metal cylinder (the perimeter is 44 cm) wrapped in foil was connected to a voltage of −300 V and placed under the nozzles with a distance of 14 cm as the collecting unit. The temperature in the enclosed space was controlled at 25 ± 2 °C and the relatively humidity was 45 ± 5%. For the fabrication process of the samples, one layer of TPU fibrous mat was prepared on the foil. GAHP was sprayed onto the fibrous mat for 1 min by a spray pen to prepare a fully GAHP decorated TPU mats. E-skin with 8 layers electrode layer was prepared by repeating the above experiment for 8 times.

2.4. Measurements

The strain and conductivity of the e-skin were tested on a tensile machine (model UTM2203, Shenzhen Sun Technology Stock Co. Ltd) and an RST5200 electrochemical workstation (Suzhou Resitest Electronic Co. Ltd., China). The morphology was analyzed by a field-emission scanning electron microscope (FE-SEM, Zeiss MERLIN Compact). The voltage, current and force of the STENG-based e-skin were measured by a KEYSIGHT DSOX2012A oscilloscope, a KEYSIGHT B2987A system electrometer and a National Instruments NI9237 Strain/Bridge Input Module, respectively.

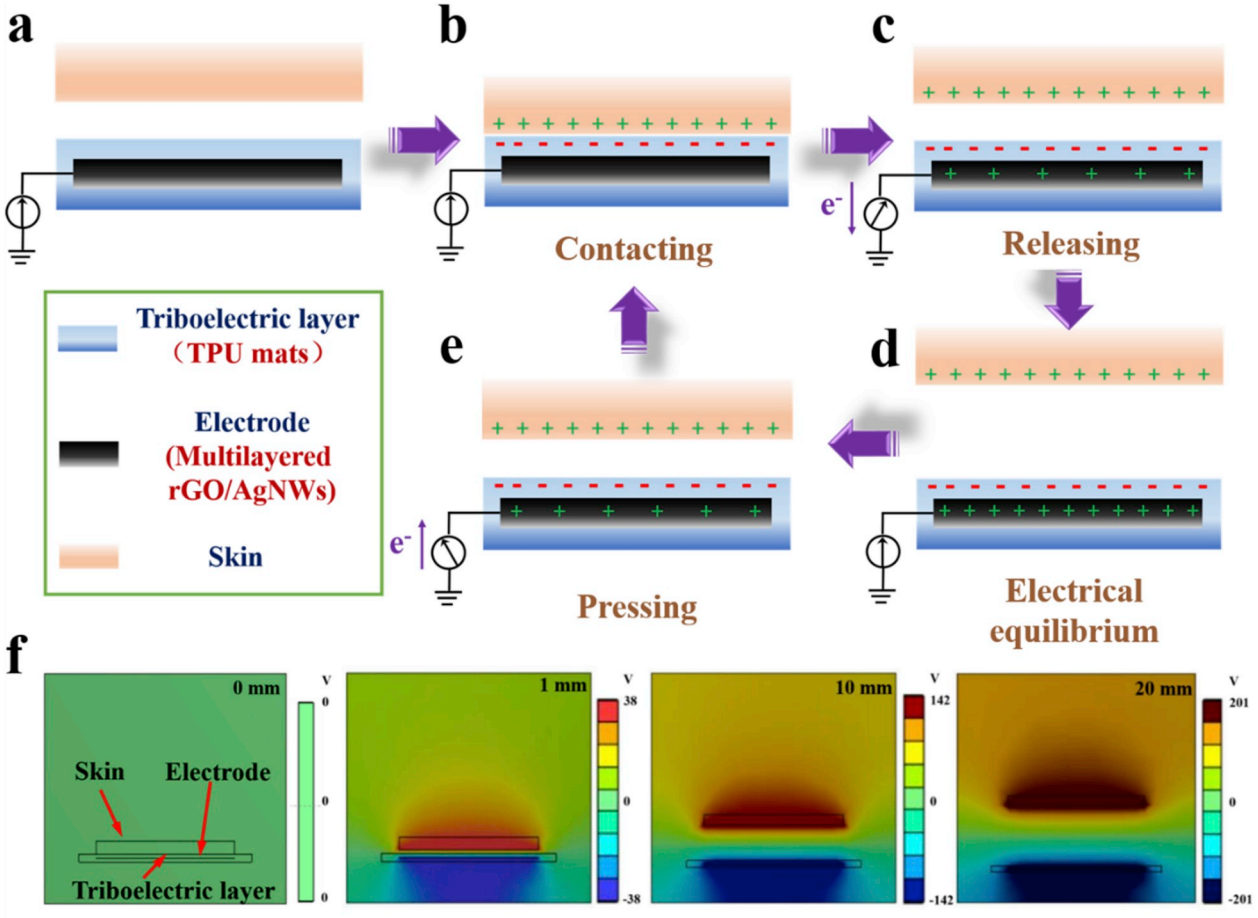

Fig. 3. (a–e) Working mechanism diagram of STENG based e-skin. (f) The simulated electric potential distribution of the STENG based e-skin.

3. Results and discussion

3.1. Characterization

In Fig. 1a, TEM images confirm that the as-prepared AgNWs are of pure morphology and high quality (diameter of ~150 nm). As shown in Fig. S2, the length of the AgNWs is about 400–500 μm, which plays a crucial role in constructing excellent conductive network. The high magnification TEM image (Fig. 1b) of rGO exhibits that the average size of a folded rGO is about 1.2–1.6 μm. Fig. 1c illustrates the equipment diagram of the fabrication of the e-skin. RGO sheets are treated under ultrasonication for 1 h and dispersed in ethanol. The AgNWs stored in ethanol are mixed equably with the rGO dispersion after stirring at a high speed. The mixed solution of AgNWs and rGO are attached to the TPU fibrous mats by spraying method, and then encapsulated by the TPU fibrous mats. Fig. 1d displays the schematic illustration for fabrication of the e-skin in different stages. The conductivity of the e-skin increases with the number of conductive layers, and 8 layers are selected due to its favorability for efficient electron transfer (Fig. S3). In short, our e-skin is consisted of 8 conductive layers and 9 layers of TPU fibrous mats. The elongation at break of the e-skin decreased slightly compared with that of the pure TPU mats, but still shows excellent stretchability (575%) (Fig. S4). The high stretchability of e-skin facilitates full contact with real human skin, which increases the amount of charge in triboelectric process, thus improving the triboelectic output performance [25]. The multi-layer AgNWs/rGO conductive network structure prevents the conductive network from being completely destroyed when the e-skin is subjected to large strain, ensuring the efficient electronic transmission. Fig. 1e displays the schematic structure of the STENG based e-skin. Our e-skin consists of two main parts: the surface TPU mats as the triboelectric and protection layers, multilayered AgNWs/rGO conductive layers as the stretchable conducting electrode. The e-skin remains completely angular on the surface of the fingers even when the fingers are bent enough in Fig. 1f, demonstrating its great flexibility and skin comfort.

Fig. 2 shows morphology of the e-skin. In Fig. 2a, the pure TPU fibers are randomly distributed and completely cover the conductive network, which improves the stretchability of the e-skin and prevents loss of sensing electrons. As shown in Fig. 2b at a higher magnification, the mats with porous structure can be observed clearly, which improves the triboelectric properties through increasing contact area between two triboelectric materials. In this paper, we set the electrospinning voltage as 26 kV, obtained uniform fibers with an average diameter of 3 μm (Fig. 2b), resulting in the highly stretchable TPU mats. Fig. 2c shows a SEM image of an un-encapsulated AgNWs/rGO conductive layer, the morphology of AgNWs and rGO can be observed clearly. The rGO sheets overlap with AgNWs, AgNWs are also randomly distributed inside and on the surface of the rGO sheets, forming synergic conductive pathways on the surface of the flexible TPU fibrous mats. Fig. 2d displays the energy dispersive spectrometer (EDS) mapping images of the conductive network, demonstrating a uniform distribution of AgNWs. As shown in Fig. S5, the resistance of the AgNWs/TPU is small (about 100 Ω), it has almost lost its conductivity under 75% strain, leading to the limit of the stretchable properties of the TENG. The resistance of AgNWs/rGO/TPU increases slowly with strain and maintains a low resistance at 200% strain, showing excellent stretchability. The excellent AgNWs/rGO conductive network can facilitate electron transfer, which is good for the stability of the e-skin. Importantly, when the conductive network is damaged under strain, many cracks appear (Fig. S6a), AgNWs with large aspect ratio tend to connect the cracks as shown in Fig. S6b, ensuring

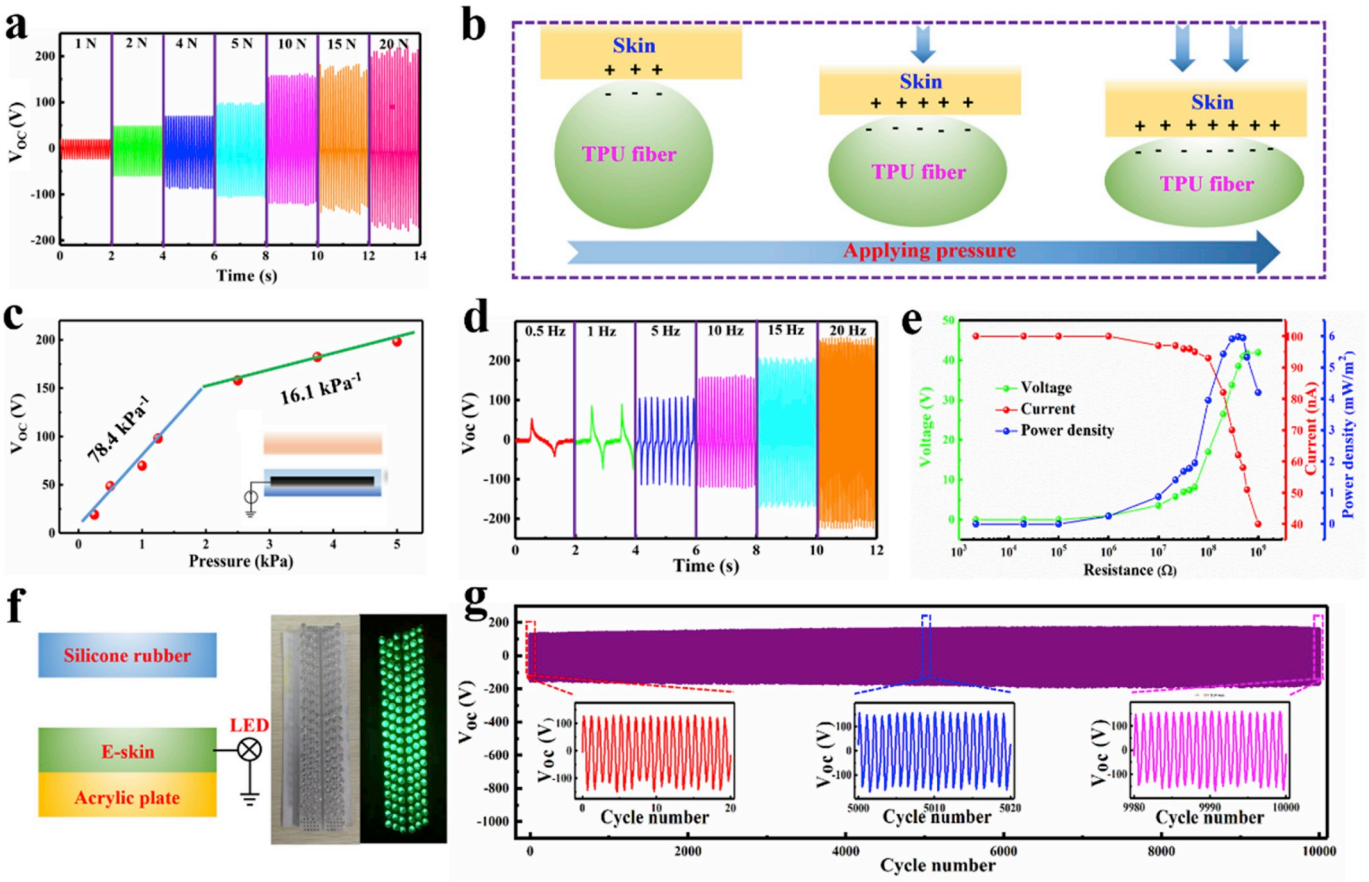

Fig. 4. Electrical output performance of the STENG based e-skin (2 × 2 cm^2). (a) V_{OC} of the e-skin with various pressures (the frequency is fixed at 10 Hz). (b) The working principle of the device output towards applied pressure. (c) The relationship between V_{OC} and pressure. The lines correspond to the linear fitting function. (d) V_{OC} of the e-skin with various frequencies (the pressure is fixed at 10 N). (e) The output performance under the resistance of 1 kΩ −1 GΩ. (f) Circuit diagram and physical pictures of e-skin lighting LEDs. (g) Long-term stability of the e-skin during 10000 working cycles (10 N, 10 Hz).

adequate electron transfer. Flexible porous TPU fibrous mats, stretchable conductive layer and multi-layered structure have guaranteed the large output performance, high stretchability and excellent stability for the e-skin.

The cross section morphology of the e-skin is illustrated in Fig. 2e, each conductive layer is covered with two layers of pure fibrous TPU mats and it forms a solidly multilayered sandwich structure, which improves the stability and durability of our e-skin. The thickness of our e-skin is about 200 μm. Here, if the thickness of the e-skin is too large, the wearing comfort will be greatly affected. Conversely, the conductive layer cannot be completely covered, resulting in a decrease in the output performance. As shown in Fig. 2c and f, after the spraying, AgNWs and rGO are coated on TPU fibers tightly, constructing continuous and stable conductive paths. In addition, the TPU mat based e-skin shows excellent air permeability. A bottle with hot water (95 °C) is then sealed by the mat based e-skin (Fig. S7a). As shown in Fig. S7b, the water vapor volatilization rate (σ) of the TPU mat based e-skin is quantitatively tested. The formula for calculating the water vapor volatilization rate is listed as follows [5]:

$$\sigma = \frac{m_0 - m_1}{m_0} \times 100\% \quad (1)$$

Where m_0 and m_1 stand for initial mass and the mass after 2 h heating at 95 °C, respectively. In Fig. S7b, after 2 h, the rest of the water of our e-skin and the open bottle are measured as 7.2 and 6 g, respectively, and the water vapor volatilization rates of our e-skin and the open bottle are 57.6% and 64.7%, respectively. The result proves that the TPU fiber mat based e-skin possesses good permeability performance of water vapor.

3.2. Working mechanism of the STENG based e-skin

The STENG based e-skin works by contact electrification and electrostatic induction [26]. Here, human skin serves as the positive triboelectric material, and TPU mats serve as the triboelectric negative material (Fig. 3a). When the human skin contacts with the TPU mats of the e-skin, because of the diverse triboelectric polarities of TPU mats and human skin, negative charges are generated at the surfaces of TPU mats, meanwhile, the positive charges are generated at the human skin (Fig. 3b). When the skin is separated from the mats, because of the electrostatic induction, the unscreened negative charges on TPU mats induce the accumulation of positive charges in AgNWs/rGO at the TPU-AgNWs/rGO interface (Fig. 3c). At the same time, the free electrons in the AgNWs/rGO composite move to the ground, producing electrical signals electrons. When the separation distance between skin surfaces and the TPU mats reached the maximum value, negative triboelectric charges on TPU mats balance well with the positive charge on the electrode (Fig. 3d). When skin surfaces and the TPU mats approach again, it works in reverse, with electrons flowing to the multilayered AgNWs/rGO conductive layers from the ground (Fig. 3e). By repeating the process of contact and separation between e-skin and the human skin, an alternating electrical signal can thus be produced [28]. Fig. 3f presents the numerical calculation results of induced voltage at different stages, which explains the process of generating electricity quantitatively. When the distance between human skin and the triboelectric layer increases from 1 to 20 mm, the potential of the triboelectric layer increases from −38 to −201 V.

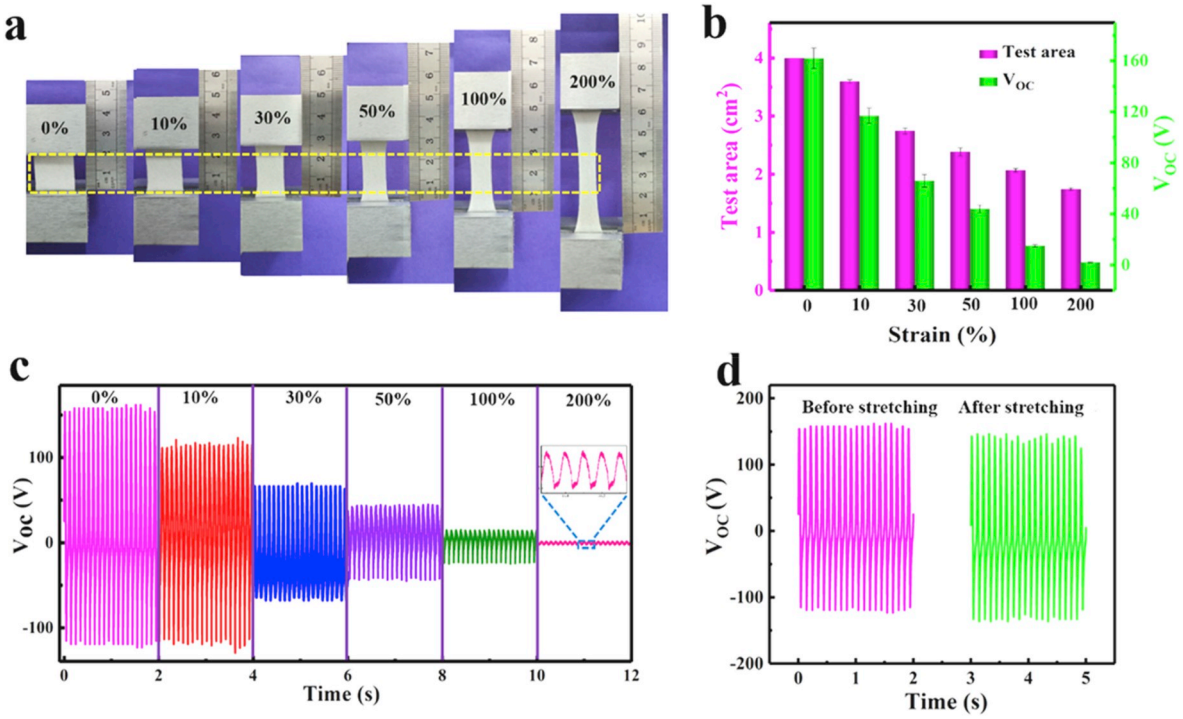

Fig. 5. (a) Physical images of e-skin stretched to different strains, (b) Effective test area and V_{OC} under different strains. (c) V_{OC} of e-skin at a series of strain ratios (10 Hz and 10 N), (d) V_{OC} of e-skin before and after stretching to 200% strain.

3.3. Sensing and stretchable capability of the self-powered e-skin

It is vitally crucial of the material to exhibit high sensitivity to various pressure, different frequencies and varying materials for self-powered e-skin [30]. To accurately test the sensitivity to pressure and frequency, we used silicone as friction material for sensitivity test. The open-circuit voltage (V_{OC}) and short-circuit current (I_{SC}) of e-skin were tested at various pressure (at a fixed frequency of 10 Hz). The V_{OC} and I_{SC} curves show fairly stable alternation towards the given pressure. Fig. 4a and Fig. S8 display the change of V_{OC} and I_{SC} towards pressure, both of the two values ascend with increase of the pressure. In Fig. 4a, the V_{OC} of e-skin increases quickly from 19 to 98 V as the applied force increases (1–5 N, contact area of 2×2 cm^2). At the pressure of 10–20 N, V_{OC} increases relatively slowly with the pressure (from 158.1 to 198.3 V), which shows that the e-skin has different response behaviors to various pressures. In Fig. 4b, as the applying pressure increases, the effective triboelectric area between the human skin and TPU fiber increases due to the deformation of the flexible TPU fiber. A larger effective contact area leads to more charge, resulting in an increase in V_{OC} [38]. As a result, increasing the applying pressure on the e-skin is an effective way to improve its output performance. On the other hand, the force of the touch can be calculated based on the V_{OC} of e-skin. To accurately analyze the sensitivity of the e-skin, the V_{OC} towards various pressures is plotted as shown in Fig. 4c. Two distinct stages are observed clearly through the linear simulations (region I 0–2 kPa and II 2–5 kPa). As shown in Fig. 4c our e-skin shows high sensitivities of 78.4 and 16.1 kPa^{-1} in region I and region II, respectively. That is, it is more sensitive at a low pressure (about 0–2 kPa). The V_{OC} and I_{SC} of e-skin at different frequencies are also studied (under the pressure of 10 N). The V_{OC} and I_{SC} increase accordingly with the operation frequency (Fig. 4d and Fig. S9). At a high frequency, the neutralization of the positive and negative charges on the friction surface is small, leading to more charges accumulating on the multilayered AgNWs/rGO conductive layers and a high electrical output. Fig. 4e displays the output properties of the e-skin under various external resistance of 1 kΩ-1 GΩ. As can be seen in Fig. 4e, the voltage of the external resistance rises while the current decreases as the resistance increases. The formula for calculating the output power density (P) is listed as follows [35]:

$$P = \frac{U^2}{RA} \tag{2}$$

Where R stands for loading resistance, A is contact area and U is output voltage of our e-skin. As shown in Fig. 4e, a good output performance of the e-skin (6 mW/m^2 at a resistance of 400 MΩ) is obtained. LED array containing 120 LEDs are fabricated as shown in Fig. 4f. Even under normal patting, the e-skin can instantaneously light up the LED array, which shows that e-skin can drive microelectronic devices. Additionally, long-term performance is also an important indicator for the e-skin in practical applications. E-skin with excellent long-term performance can enlarge the popularity and reduce the usage cost remarkably. As shown in Fig. 4g, our e-skin maintains the stability even it was pressed and released continuously for 10000 cycles, which shows an excellent working stability. Humidity and temperature stability are important parameters for the wearable electronics, especially for the devices contacting with skin directly. As shown in Fig. S10a, our e-skin in this study can operate under a high relative humidity of 80%, exhibiting a good performance to humidity. The V_{OC} of e-skin changes weakly with the variation of temperature, showing excellent temperature stability (Fig. S10b).

As a wearable self-powered device, it requires the ability to generate electricity under various extreme deformation conditions [45]. As shown in Fig. S11, in order to study the change of electrode layer when it is stretched, the relationship between conductivity and strain is also tested. When the e-skin is stretched, the conductivity of the electrode layer decreases as the strain rises. Due to excellent stretchability of the TPU mats and stability of the AgNWs/rGO conductive network against strain, our e-skin still possesses good electron transport capacity despite being stretched to 200% strain. Moreover, after the strain is released, the electrical conductivity of our e-skin can return to the original state, which verifies great advantage of e-skin in stretchability. Fig. S12 shows the resistance of the AgNWs/rGO electrode after being stretched and released for 100 times under 200% strain. The initial resistance of the

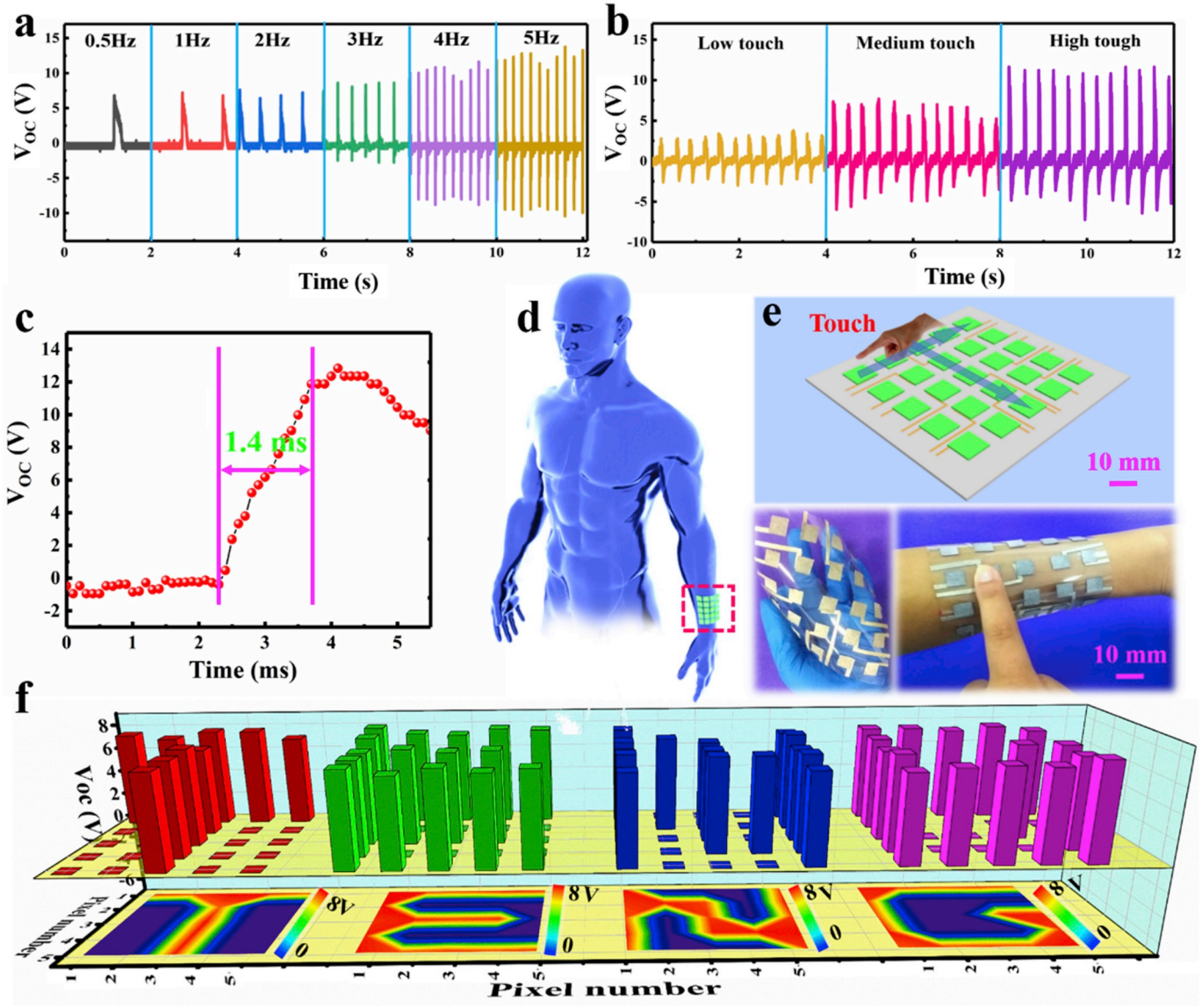

Fig. 6. Applications of the self-powered e-skin in tactile sensing and energy harvesting. V_{OC} of the single e-skin with different frequencies (a) and strengths (b) of finger touch. (c) The response time of the e-skin under 5 Hz. (d) Photographs of the e-skin array attached to the forearm state. (e) Schematic description of a flexible tactile sensing e-skin array with 5 × 5 pixels. (f) The movement track index finger and the output voltage mapping.

electrode (before stretch) is 496 Ω, the resistance of the electrode after being stretched 100 times under 200% strain is 913 Ω. It is worth noting that the resistance of the electrode tends to be stable after 10 stretching-releasing cycles, which is good to the stability of the e-skin in long-term use. As shown in Fig. 5a, a 2 × 2 cm^2 e-skin was attached to the stretching device and stretched to 200% strain, and it can almost return to its initial length after being stretched to 200% strain (Fig. S13). The V_{OC} of the e-skin under different strains was tested. It should be noted that the length of the tested friction area of the e-skin is constant (2 cm) when stretched, while the width rises gradually as the strain increases, which results in the reduction of the effective triboelectric area. Fig. 5b shows the changes of effective test area and V_{OC} under different strains. As the strain increases, the test area of the e-skin decreases from 4 to 1.75 cm^2. The variations of voltage and test area towards strain are similar, which indicates that the V_{OC} drop of the e-skin is related to the decrease of the test area. The V_{OC} decreases with the increase of e-skin strain, that is because the path of electron transfer is elongated and the triboelectric area decreases, nevertheless, the stable V_{OC} signals can still generate even under 200% strain as shown in Fig. 5b. Importantly, after the strain was completely released, our e-skin could maintain the excellent V_{OC} output capability, just as the initial sample. That is because the electrode layers are wrapped tightly by the TPU fibrous mats in the preparation. As shown in Fig. S14a, although the e-skin is stretched and released for 1000 times at a large strain of 200%, its mechanical properties are not significantly reduced. After the e-skin is stretched and released for 1000 times, the V_{OC} of our e-skin is then tested at 45% relative humidity and 25 °C. The results display that the e-skin could still harvest energy efficiently, showing excellent enduring ability (Fig. S14b). The e-skin can effectively harvest energy at 200% strain, showing excellent stretchability and promising prospects in the field of flexible energy supply, such as flexible electronics, soft robots and so on. On the other hand, the differences in V_{OC} of the e-skin under different strains can be used to sense deformation, which has great potential in human motion monitoring, health care and human-machine interaction.

3.4. Applications of the self-powered e-skins

Our e-skin is then applied to assemble multifunctional wearable devices for tactile sensing and energy harvesting. The e-skin (1 × 1 cm^2)

is attached to human skin to sense touch of fingers and harvest electrical energy. The V_{OC} of e-skin increases as the finger touch frequency increases, demonstrating sensitive sensing of touch at different frequencies (Fig. 6a). To further test the feasibility of the e-skin in strength of its touch, the volunteers used three different forces to touch the e-skin (low touch, medium touch and high touch, respectively). Fig. 6b displays three different curves with peaks of 3, 7 and 12 V, respectively, proving that the e-skin is extremely sensitive to strength of touch. When the e-skin is touched, the frequency of the touch can be estimated by calculating the time between the two adjacent peaks of electrical signal. In daily life, the stimuli by the e-skin are often low-frequency. As shown in Fig. 6a, the output performance of our e-skin is affected weakly under a low frequency of 0.5–3 Hz.

When stimulated by the outside things, the quick response of e-skin facilitates people or robots to make judgments and actions quickly [51, 57]. Interestingly, response time of our e-skin is related to frequency. The response time of our e-skin under 5 Hz is 1.4 ms as shown in Fig. 6c, leaving enough time for human to deal with the stimulus. In addition, in order to solve the detection limitation of a single sensing unit and provide comprehensive information, multiple single sensing units are integrated, which forms a wearable self-powered e-skin array and can realize a mapping of touch in two-dimensional area. On the basis of the single e-skin (1×1 cm^2), a 5×5 tactile sensing e-skin array on polycarbonate (PC) film was fabricated, which can be comfortably and easily applied onto human skin (Fig. 6d and e). Fig. 6f illustrates that the object static contact position with the surface of the e-skin array and the finger motion trajectory ("T", "E" "N" and "G", respectively) can be accurately monitored. These results prove that our e-skin is capable of performing skin sensing to mapping external stimulations and harvest electrical energy, enabling potential applications of human-machine interaction.

4. Conclusions

In summary, a STENG based e-skin with multilayered flexible fibrous TPU mats and AgNWs/rGO synergic conductive network is fabricated by electrospinning and spraying technique. A high stretchability (200% strain) of the e-skin has been achieved by designing a synergic rGO/AgNWs conductive network in multilayered TPU fibrous mats. The e-skin can convert the energy produced by human movement into electrical energy steadily with an instantaneous peak voltage of 202.4 V and energy density of 6 mW/m^2 (size of 2×2 cm^2). In addition, the e-skin possesses a high sensitivity (78.4 kPa^{-1}) as well as a fast response time (1.4 ms) towards pressure, exhibiting the potential prospect as a high performance tactile sensor. On the basis of the power supply ability and excellent sensing performances, the e-skin is capable of sensing strength and trajectory of mechanical stimuli in self-powered manner in real time. The ultra-stretchable e-skin and energy conversion system show promising applications in internet of things, soft robots and human-machine interaction.

Declaration of competing interest

The authors declare that they have no known competing financial interests or personal relationships that could have appeared to influence the work reported in this paper.

Acknowledgements

The authors acknowledge the financial support of this research by National Natural Science Foundation of China (51773183, U1804133, 51603193, 11572290), National Natural Science Foundation of China-Henan Province Joint Funds (U1604253), Henan Province University Innovation Talents Support Program (20HASTIT001), Innovation Team of Colleges and Universities in Henan Province (20IRTSTHN002).

Appendix A. Supplementary data

Supplementary data to this article can be found online at https://doi.org/10.1016/j.nanoen.2020.104546.

References

[1] X. Yu, Z. Xie, Y. Yu, J. Lee, A. Vazquez-Guardado, H. Luan, J. Ruban, X. Ning, A. Akhtar, D. Li, B. Ji, Y. Liu, R. Sun, J. Cao, Q. Huo, Y. Zhong, C. Lee, S. Kim, P. Gutruf, C. Zhang, Y. Xue, Q. Guo, A. Chempakasseril, P. Tian, W. Lu, J. Jeong, Y. Yu, J. Cornman, C. Tan, B. Kim, K. Lee, X. Feng, Y. Huang, J.A. Rogers, Nature 575 (2019) 473–479.
[2] L. Wang, W.A. Daoud, Nano Energy 66 (2019) 104080.
[3] J. Yang, J. Mun, S. Kwon, S. Park, Z. Bao, S. Park, Adv. Mater. (2019), e1904765.
[4] D. Wen, X. Liu, H. Deng, D. Sun, H. Qian, J. Brugger, X. Zhang, Nano Energy 66 (2019) 104123.
[5] Y. Jia, X. Yue, Y. Wang, C. Yan, G. Zheng, K. Dai, C. Liu, C. Shen, Compos. B Eng. 183 (2019) 107696.
[6] L. Wang, L. Wang, Y. Zhang, J. Pan, S. Li, X. Sun, B. Zhang, H. Peng, Adv. Funct. Mater. 28 (2018) 1804456.
[7] T. Araki, T. Uemura, S. Yoshimoto, A. Takemoto, Y. Noda, S. Izumi, T. Sekitani, Adv. Mater. (2019) 1902684.
[8] Y. Kim, A. Chortos, W. Xu, Y. Liu, J.Y. Oh, D. Son, J. Kang, A.M. Foudeh, C. Zhu, Y. Lee, S. Niu, J. Liu, R. Pfattner, Z. Bao, T.-W. Lee, Science 360 (2018) 998–1003.
[9] S. Wang, J. Xu, W. Wang, G.N. Wang, R. Rastak, F. Molina-Lopez, J.W. Chung, S. Niu, V.R. Feig, J. Lopez, T. Lei, S.K. Kwon, Y. Kim, A.M. Foudeh, A. Ehrlich, A. Gasperini, Y. Yun, B. Murmann, J.B. Tok, Z. Bao, Nature 555 (2018) 83–88.
[10] J.C. Yang, J. Mun, S.Y. Kwon, S. Park, Z. Bao, S. Park, Adv. Mater. (2019), e1904765.
[11] D. Son, J. Kang, O. Vardoulis, Y. Kim, N. Matsuhisa, J.Y. Oh, J.W. To, J. Mun, T. Katsumata, Y. Liu, A.F. McGuire, M. Krason, F. Molina-Lopez, J. Ham, U. Kraft, Y. Lee, Y. Yun, J.B. Tok, Z. Bao, Nat. Nanotechnol. 13 (2018) 1057–1065.
[12] Y. Liu, X. Shi, S. Liu, H. Li, H. Zhang, C. Wang, J. Liang, Y. Chen, Nano Energy 63 (2019) 103898.
[13] Y. Yu, Y. Zhai, Z. Yun, W. Zhai, X. Wang, G. Zheng, C. Yan, K. Dai, C. Liu, C. Shen, Adv. Electron. Mater. (2019) 1900538.
[14] Y. Zhai, Y. Yu, K. Zhou, Z. Yun, W. Huang, H. Liu, Q. Xia, K. Dai, G. Zheng, C. Liu, C. Shen, Chem. Eng. J. (2019) 122985.
[15] W. Liu, Z. Wang, G. Wang, G. Liu, J. Chen, X. Pu, Y. Xi, X. Wang, H. Guo, C. Hu, Z. L. Wang, Nat. Commun. 10 (2019) 1426.
[16] W. Xiong, K. Hu, Z. Li, Y. Jiang, Z. Li, Z. Li, X. Wang, Nano Energy 66 (2019) 104149.
[17] L. Wang, L. Wang, Y. Zhang, J. Pan, S. Li, X. Sun, B. Zhang, H. Peng, Adv. Funct. Mater. 28 (2018) 1804456.
[18] T. Li, J. Zou, F. Xing, M. Zhang, X. Cao, N. Wang, Z.L. Wang, ACS Nano 11 (2017) 3950–3956.
[19] D. Liu, X. Yin, H. Guo, L. Zhou, X. Li, C. Zhang, J. Wang, Z.L. Wang, Sci. Adv. 5 (2019), eaav6437.
[20] S. Li, J. Wang, W. Peng, L. Lin, Y. Zi, S. Wang, G. Zhang, Z.L. Wang, Adv. Energy Mater. 7 (2017) 1602832.
[21] Y. Jie, H. Zhu, X. Cao, Y. Zhang, N. Wang, L. Zhang, Z.L. Wang, ACS Nano 10 (2016) 10366–10372.
[22] X. Cao, Y. Jie, N. Wang, Z.L. Wang, Adv. Energy Mater. 6 (2016) 1600665.
[23] J. Luo, Z. Wang, L. Xu, A.C. Wang, K. Han, T. Jiang, Q. Lai, Y. Bai, W. Tang, F. R. Fan, Z.L. Wang, Nat. Commun. 10 (2019) 5147.
[24] Y. Jie, X. Jia, J. Zou, Y. Chen, N. Wang, Z.L. Wang, X. Cao, Adv. Energy Mater. 8 (2018) 1703133.
[25] Y. Peng, J. Lu, D. Peng, W. Ma, F. Li, Q. Chen, X. Wang, J. Sun, H. Liu, C. Pan, Adv. Funct. Mater. (2019) 1905051.
[26] Y. Jie, Q. Jiang, Y. Zhang, N. Wang, X. Cao, Nano Energy 27 (2016) 554–560.
[27] Y. Cheng, D. Wu, S. Hao, Y. Jie, X. Cao, N. Wang, Z.L. Wang, Nano Energy 64 (2019) 103907.
[28] X. Cao, M. Zhang, J. Huang, T. Jiang, J. Zou, N. Wang, Z.L. Wang, Adv. Mater. 30 (2018) 1704077.
[29] Y. Lai, J. Deng, R. Liu, Y. Hsiao, S. Zhang, W. Peng, H. Wu, X. Wang, Z.L. Wang, Adv. Mater. 30 (2018), e1801114.
[30] Y. Pang, S. Chen, Y. Chu, Z.L. Wang, C. Cao, Nano Energy 66 (2019) 104131.
[31] Y. Lai, J. Deng, S. Niu, W. Peng, C. Wu, R. Liu, Z. Wen, Z.L. Wang, Adv. Mater. 28 (2016) 10024–10032.
[32] C. Zhang, Z. Guo, X. Zheng, X. Zhao, H. Wang, F. Liang, S. Guan, Y. Wang, Y. Zhao, A. Chen, G. Zhu, Z.L. Wang, Adv. Mater. (2019) 1904988.
[33] P. Jiang, L. Zhang, H. Guo, C. Chen, C. Wu, S. Zhang, Z.L. Wang, Adv. Mater. 31 (2019) 1902793.
[34] K. Dong, X. Peng, Z.L. Wang, Adv. Mater. (2019), e1902549.
[35] F. Peng, D. Liu, W. Zhao, G. Zheng, Y. Ji, K. Dai, L. Mi, D. Zhang, C. Liu, C. Shen, Nano Energy 65 (2019) 104068.
[36] Y. Lai, J. Deng, S. Zhang, S. Niu, H. Guo, Z.L. Wang, Adv. Funct. Mater. 27 (2017) 1604462.
[37] W. Xiong, K. Hu, Z. Li, Y. Jiang, Z. Li, Z. Li, X. Wang, Nano Energy 66 (2019) 104149.
[38] H. Qiu, W. Song, X. Wang, J. Zhang, Z. Fan, M. Yu, S. Ramakrishna, Y. Long, Nano Energy 58 (2019) 536–542.
[39] Z. Zhang, Y. Bai, L. Xu, M. Zhao, M. Shi, Z.L. Wang, X. Lu, Nano Energy 66 (2019) 104169.

[40] S. Chun, C. Pang, S.B. Cho, Adv. Mater. (2019) 1905539.
[41] K. Parida, G. Thangavel, G. Cai, X. Zhou, S. Park, J. Xiong, P.S. Lee, Nat. Commun. 10 (2019) 2158.
[42] J. Chen, B. Chen, K. Han, W. Tang, Z.L. Wang, Adv. Mater. Technol. 4 (2019) 1900337.
[43] Y. Bai, L. Xu, C. He, L. Zhu, X. Yang, T. Jiang, J. Nie, W. Zhong, Z.L. Wang, Nano Energy 66 (2019) 104117.
[44] Z. Wu, B. Zhang, H. Zou, Z. Lin, G. Liu, Z.L. Wang, Adv. Energy. Mater. 9 (2019) 1901124.
[45] Z. Lin, B. Zhang, H. Guo, Z. Wu, H. Zou, J. Yang, Z.L. Wang, Nano Energy 64 (2019) 103908.
[46] J. Tao, R. Bao, X. Wang, Y. Peng, J. Li, S. Fu, C. Pan, Z.L. Wang, Adv. Funct. Mater. 29 (2018) 1806379.
[47] X. Zhu, X. Meng, S. Kuang, X. Wang, C. Pan, G. Zhu, Z.L. Wang, Nano Energy 41 (2017) 387–393.
[48] Z. Bai, Z. Zhang, J. Li, J. Guo, Nano energy 65 (2019) 104012.
[49] L. Lin, Y. Xie, S. Wang, W. Wu, S. Niu, X. Wen, Z.L. Wang, ACS Nano 7 (2013) 8266–8274.
[50] H. Zhang, W. Niu, S. Zhang, ACS Appl. Mater. Interfaces 10 (2018) 32640–32648.
[51] S. Zhao, J. Wang, X. Du, J. Wang, R. Cao, Y. Yin, X. Zhang, Z. Yuan, Y. Xing, D.Y. H. Pui, C. Li, ACS Appl. Energy Mater. 1 (2018) 2326–2332.
[52] M. Lin, J. Xiong, J. Wang, K. Parida, P. Lee, Nano Energy 44 (2018) 248–255.
[53] H. Li, T. Sinha, J. Lee, J. Oh, Y. Ahn, J. Kim, Adv. Mater. Interfaces 5 (2018) 1800635.
[54] Y. Yang, Z. Cao, P. He, L. Shi, G. Ding, R. Wang, J. Sun, Nano Energy 66 (2019) 104134.
[55] Y. Tang, H. Zhou, X. Sun, N. Diao, J. Wang, B. Zhang, C. Qin, E. Liang, Y. Mao, Adv. Funct. Mater. (2019) 1907893.
[56] X. Pu, M. Liu, X. Chen, J. Sun, C. Du, Y. Zhang, J. Zhai, W. Hu, Z.L. Wang, Sci. Adv. 3 (2017), e1700015.
[57] Q. Hua, J. Sun, H. Liu, R. Bao, R. Yu, J. Zhai, C. Pan, Z.L. Wang, Nat. Commun. 9 (2018) 244.

Kangkang Zhou received his B.S. degree in Material Science and Engineering from Zhengzhou University. Now he is a postgraduate student in Zhengzhou University. His current research interest is flexible and self-powered electronic skin.

Yi Zhao received his B.S. degree in Material Science and Engineering from Hubei University of technology. He is now a postgraduate student of Zhengzhou University. His current research interests focus on electronic skin for energy collection and flexible self-powered electronics.

Xiupeng Sun is an undergraduate student in School of Physics and Engineering at Zhengzhou University. His major is Physics. His research interests are related to the flexible electronic devices and smart sensors.

Zuqing Yuan received his B.S. degree from the Department of Materials Science and Engineering from University of Science and Technology Beijing in 2014. Then he earned Ph.D. degree from Beijing Institute of Nanoenergy and Nanosystems in 2019. His main research interests focus on the smart devices for energy harvesting and flexible electronics.

Guoqiang Zheng received his M.S. degree in Material Processing Engineering from Zhengzhou University, China in 2004, and Ph.D. degree in Material Processing Engineering from Sichuan University, China in 2007. He was invited to Zhengzhou University, China as a lecturer in 2007, and then got promoted to associate professor and full professor in 2008 and 2013 respectively. Now, he is the distinguished professor of Henan province. His current research interest is polymer functionalization via melt processing methods.

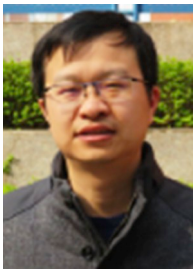

Kun Dai received his B.S. and Ph.D. in College of Polymer Science and engineering from Sichuan University, China in 2005 and 2011, respectively. From 2008 to 2010, he studied at University of California, Los Angeles, under the supervision of Prof. Yunfeng Lu. Now he is promoted to full professor in Zhengzhou University. His current main research interests include structure and properties of conductive polymer composites and flexible wearable electronics.

Liwei Mi received his B.S., M.S. and Ph.D. from Zhengzhou University. In 2014, he worked as a professor of materials science in Zhongyuan University of Technology. His current research interest focuses on the controllable preparation and performance study of functionalized micro/nanomaterials. He has published over 110 peer-reviewed articles and holds 15 authorized invention patents of China.

Caofeng Pan received his B.S. (2005) and Ph.D. degree (2010) in Materials Science and Engineering from Tsinghua University, China. He then joined the Georgia Institute of Technology as a postdoctoral fellow. He is currently a professor and a group leader at Beijing Institute of Nanoenergy and Nanosystems, Chinese Academy of Sciences since 2013. His main research interests focus on the fields of piezotronics/piezo-phototronics for fabricating new electronic and optoelectronic devices, and self-powered nanosystems.

Chuntai Liu, currently a professor of the National Engineering Research Center for Advanced Polymer Processing Technology (NERC) of Zhengzhou University, he obtained his B.S.and M.S. respectively from Beijing University (1987) and Xian Jiaotong University (1993) and his Ph.D. from Zhengzhou University (2003). He worked as a visiting scholar at Ohio State University (2006–2007). He now serves as the deputy director of NERC of Zhengzhou University. His research focuses on multifunctional polymer composites including the relationship of processing-microstructure-properties.

Changyu Shen, currently a professor of National Engineering Research Center for Advanced Polymer Processing Technology (NERC) of Zhengzhou University and an academician of Chinese Academy of Sciences, obtained his M.S. and Ph.D. from Dalian University of Technology in 1987 and 1990 respectively. Shen has made original and innovative contributions to numerical simulation of plastic forming process, optimization design and manufacture of plastic mold as well as structured and lightweight composites. He now serves as the director of NERC of Zhengzhou University.